Appl. Phys. B 70, 889–893 (2000) / Digital Object Identifier (DOI) 10.1007/s003400000220

Applied Physics B
Lasers
and Optics

Lamb-dip stabilized 543-nm He-Ne lasers and isotope shift of Ne $3s_2 \rightarrow 2p_{10}$ transition

W.-Y. Cheng, J.-T. Shy

Department of Physics, National Tsing Hua University, Hsinchu, Taiwan 300, ROC
(Fax: +886-35/723-052, E-mail: d827312@phys.nthu.edu.tw; shy@phys.nthu.edu.tw)

Received: 31 March 1999/Revised version: 1 November 1999/Published online: 24 March 2000 –

Abstract. Internal-mirror 543-nm He-^{20}Ne and He-^{22}Ne lasers are frequency-stabilized to the Lamb-dip of their tuning curves. Frequency stability of 2×10^{-11} and frequency resettability of 4×10^{-9} (or 2 MHz) are achieved. The absolute frequencies of the two lasers are determined by frequency-comparing with an iodine-stabilized 543-nm laser. The isotope shift between ^{20}Ne and ^{22}Ne is measured to one order of magnitude more accurately than the previous result, and the specific-mass-shift for Ne $3s_2 \rightarrow 2p_{10}$ transition is also determined.

PACS: 35; 42.55.H; 42.80

Early in 1963, the power saturation dip of a single-mode gas laser, which is referred to as "Lamb-dip" now, was theoretically predicted [1, 2] and experimentally realized [3]. In 1965, Shimoda and Javan first successfully frequency-stabilized a 1.15-μm He-Ne laser to the center of the Lamb-dip and they also gave a detail analysis on such a system [4]. Later, Hall pointed out that the Lamb-dip stabilized lasers are not suitable for primary wavelength standards due to the pressure shift and asymmetric line shape in the Lamb-dip [5]. However, the Lamb-dip stabilized lasers can serve as the secondary wavelength standards for some metrology applications since they have sufficient long-term and short-term stability (10^{-8} resettability and 10^{-11} stability typically [5, 6]). Besides, Lamb-dip stabilized He-Ne lasers are handy and convenient compared with the corresponding primary wavelength standard lasers. For example, some applications used the Lamb-dip stabilized lasers together with a high-finesse Fabry–Pérot etalon as the absolute frequency references [7–11]. Therefore, detailed studies and the absolute frequency measurements of the Lamb-dip stabilized lasers are significant for generalizing their applications.

The first iodine-stabilized 543-nm He-Ne laser system was reported in 1989 [12], and many efforts on such a wavelength standard laser system have been performed since then [13–18]. The iodine-stabilized 543-nm He-Ne laser was adopted as a recommended wavelength standard in 1992 [19]. However, the complicated configurations of those systems limited its applications and only one inter-comparison for the iodine-stabilized 543-nm lasers was performed up to now. Recently we reported a compact and highly stable iodine-stabilized 543-nm He-Ne laser system [19] which is easy to maintain. Hence it is worthwhile to investigate the corresponding secondary wavelength standard laser systems, such as the Lamb-dip stabilized lasers for extending the use of such a wavelength standard.

On the other hand, as the Lamb-dip stabilized He-^{20}Ne, He-^{22}Ne lasers have the frequencies very close to their atomic transition centers, beat frequency measurements between the Lamb-dip stabilized He-^{20}Ne, He-^{22}Ne lasers thus provide a good way to determine the isotope shift between ^{20}Ne and ^{22}Ne atoms precisely. The determined isotope shift is important in searching the specific-mass-shift (SMS) of Ne atom which is of interest to the nuclear and atomic physicists in the understanding of the nuclear structure and the J-dependence of the electronic wavefunction of the excited state of Ne atom. In the past, the isotope shifts of the Ne atom at the 3391-nm [20], 1523-nm [6], 1152-nm [21], and 633-nm [22] laser transitions have been determined by the Lamb-dips of the corresponding He-Ne lasers.

In this paper, we report on our results of the Lamb-dip stabilization of internal-mirror 543-nm He-Ne lasers. We have constructed two Lamb-dip stabilized 543-nm He-Ne lasers with a frequency stability of 2×10^{-11} (normalized to 1 Hz bandwidth) and a frequency resettability of 4×10^{-9}. We have also determined the frequencies of the two Lamb-dip stabilized lasers of different isotopes (^{20}Ne and ^{22}Ne) with respect to an iodine-stabilized laser. From this, we can deduce the isotope shift (1014 ± 5 MHz) between ^{20}Ne and ^{22}Ne in $3s_2 \rightarrow 2p_{10}$ (Paschen notation) transition and also its specific-mass-shift (SMS) (253 ± 5 MHz). Our result of isotope shift is one order of magnitude better than Gerstenberger, Drobshoff, and Sheng's work [23] in accuracy. The previous results for the isotope shift of Ne $3s_2 \rightarrow 2p_4$ 633-nm laser transition [22, 24] yield an averaged SMS of -291 ± 9 MHz. The

large discrepancy between those two results on SMS supports the J-dependence of SMS [25]

1 Experimental setup

The 543-nm laser tubes used in our experiment are Melles Griot model LGR-024 (filled with ^{22}Ne) and LGR-024-S (filled with ^{20}Ne). For controlling the laser cavity length, we wrap a thin-film heating tape and attach a piezoelectric transducer (PZT) tube onto each laser tube. The laser tube is put into an aluminum tube and it is then enclosed in a wooden box to reduce the thermal perturbations.

The mode spacing of our lasers is about 750 MHz and usually their outputs have two longitudinal modes with linear polarization orthogonal to each other. A weak magnetic field of equal strength is applied to both lasers to suppress the polarization flipping [26, 27]. In order to avoid the mode-coupling effect when the laser frequency is tuned to the Lamb-dip region, we increase the laser threshold by slightly misaligning the laser back-end mirror to achieve single-frequency operating around the Lamb-dip region. After those adjustments the lasers yield 80 μW output power at maximum and have about 260 MHz single-frequency tuning range near the center of the gain profile. That is, through the most part of Lamb-dip region, the lasers are single-mode operation. Outside the Lamb-dip region, the lasers still behave as two-mode operation and a polarizing beamsplitter can be used to select one longitudinal mode which has a tuning range about 1.5 GHz.

The experimental setup for Lamb-dip stabilization and frequency measurement is shown in Fig. 1. The Faraday isolator FI is used to prevent the optical feedback effect and also to select one longitudinal mode. The polarizing beamsplitter PBS and the $\lambda/4$ waveplate WP are used to direct the retro- reflection beam from the moving mirror or the end mirror onto the photodiode PD. The light ($\approx 1\%$) of the main laser output reflected by the PBS is used for beating against a two-mode stabilized laser. The beat note is detected using an avalanche photodiode APD and monitored by a HP spectrum analyzer. When the laser beam is reflected by the moving mirror, we obtain the power profile of selected mode directly. Figure 2 shows the typical one-mode power profile vs. frequency when the laser beam is reflected from the moving mirror. When the laser beam is reflected by the end mirror, we obtain the saturation spectrum of the iodine. The lens ($f = 20$ cm) is used to increase the laser intensity in the iodine cell.

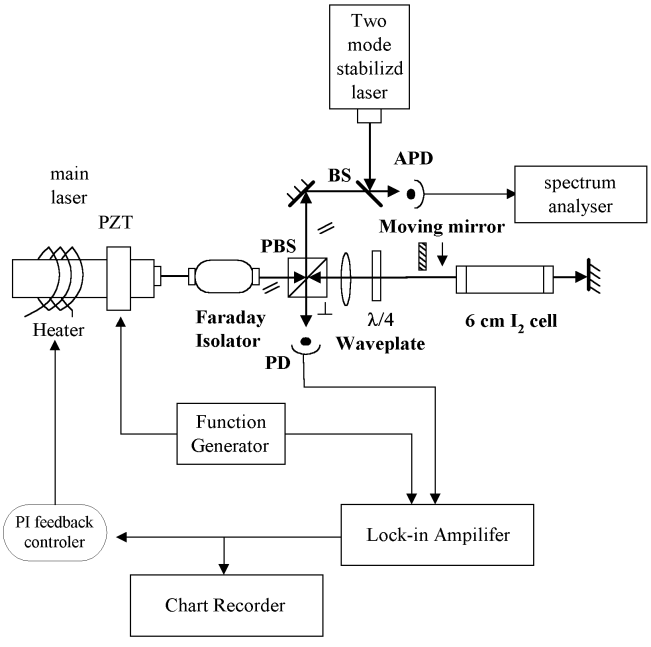

Fig. 1. A schematic diagram of the Lamb-dip stabilized laser and frequency measurement. PBS: polarization beamsplitter. PD: photo-diode. APD: avalanche photo-diode. BS: beamsplitter

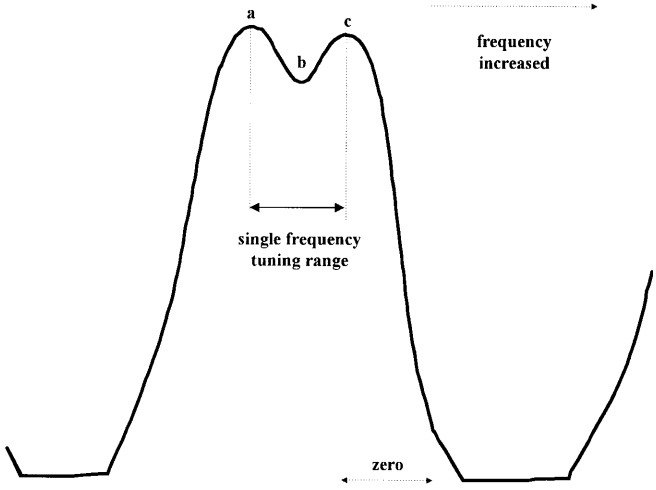

Fig. 2. Typical Lamb-dip profile of He-^{20}Ne laser. The maximum output power is about 80 μW. The depth of dip is about 10% of the maximum power. The points a, b, and c correspond to the three zero-crossings of the first-harmonic signal in Fig. 3

For stabilizing the laser frequency to the center of the Lamb-dip (point b in Fig. 2), we modulate the laser frequency at 32 kHz with a modulation width of 15 to 30 MHz through the PZT glued on the laser tube. The error signal is obtained by the first-harmonic demodulation technique using a lock-in amplifier and it is fed to the heating tape through a conventional proportional-integral controller.

The frequency of the Lamb-dip laser is measured by the following procedures. First, we stabilize the laser to one of the iodine hyperfine peaks following the procedures in [14] (the moving mirror is removed from the optical path in Fig. 1), and record the beat frequency against the two-mode stabilized 543-nm laser. Second, by inserting the moving mirror in the optical path, we stabilize the main laser to the center of the Lamb-dip, then record the beat frequency against the two-mode stabilized laser again. Lastly, we repeat the first step to make sure that the frequency of the two-mode stabilized laser does not drift during the measuring time. The two-mode stabilized laser, has frequency stability better than 1×10^{-10} and 10 MHz frequency drift in fifteen days by comparing with an iodine-stabilized 543-nm He-Ne laser. For the iodine stabilization, the He-^{20}Ne laser is stabilized to the hyperfine component a_9 of R(12)106-0 iodine line, whereas He-^{22}Ne laser is stabilized to b_{15} component of R(106)28-0 iodine line. The cold-finger temperature of the 6-cm-long iodine cell is set at 0 °C which is recommended by CIPM [28].

2 Experimental results

Figure 2 shows the typical Lamb-dip profile for the He-^{20}Ne laser. The maximum laser output power is about 80 μW and the depth of the dip is about 10%. The profile is slightly asymmetric and the local maximum at the lower frequency side is higher than that at the higher frequency side. However, the Lamb-dip profile of the He-^{22}Ne laser shows more pronounced asymmetry and, the local maximum at the lower frequency side is also higher than that at the higher frequency side. This indicates the frequency of the Lamb-dip center is higher than the center frequency of the power background.

There are many mechanisms for the asymmetric lineshape. It can be caused by the gas-lensing-caused asymmetric cavity loss [29], by the soft-collision effect [4, 30, 31], by the impurity of the isotope [3, 32], and by the nonlinear frequency response for the modulation [33]. Since both of our lasers have the same structure and output power, and the modulation width far smaller than the dip-width (defined later), we presume the impurity of the isotope is the major reason for the larger asymmetry in the Lamb dip of the He-^{22}Ne laser. The transition frequency of ^{22}Ne is higher than ^{20}Ne and the 543-nm Ne laser transition is very weak. Therefore, a small amount of ^{20}Ne will redshift the peak of the power background a lot.

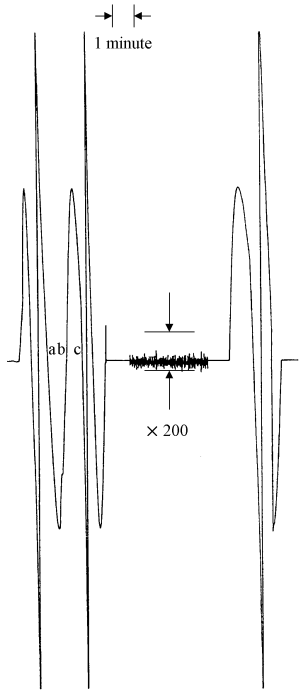

Fig. 3. Typical first-harmonic signal of Fig. 2. Laser is frequency-stabilized at b, and the signal-to-noise ratio is about 11 000 normalized to 1 Hz bandwidth. The dip-width is defined as half of the measured frequency difference f_{ac}. The dip-widths are measured to be 199 MHz and 209 MHz for our ^{20}Ne and ^{22}Ne laser, respectively

2.1 Frequency stability and resettability

A typical error signal obtained by the first-harmonic demodulation technique is shown in Fig. 3, which also shows the fluctuation of the error signal after the laser is locked. The frequency stability can be estimated by dip-width/(S/N), in which the dip-width is the linewidth of the Lamb-dip and S/N is the signal-to-noise ratio after the laser is locked. The dip-width ($\approx$ 200 MHz) is estimated as half of the frequency difference between the two zero-crossing points a and c in Fig. 3 and the S/N (signal-to-noise ratio) can be measured from Fig. 3 directly. Therefore, we obtained a frequency stability about 10^{-11} normalized to 1 Hz bandwidth (the bandwidth of our chart recorder is 2.7 Hz). The resettability is defined [6, 16] as the variation of the absolute frequency of a laser in a period of time. Therefore, the resettability here is an index for the accuracy of the measured absolute frequency of the Lamb-dip stabilized laser. Here, we obtain the resettability of our Lamb-dip stabilized lasers by frequency-comparing with an iodine-stabilized laser, and frequency variation less than 2 MHz fluctuation was observed for a period of fifteen days. In comparison, our Lamb-dip stabilized lasers show better long-term stability than our two-mode stabilized laser which has 10 MHz fluctuation for the same period of time.

2.2 Absolute frequencies of the Lamb-dips

With the recommended frequency in [28], the absolute frequencies of the Lamb-dip stabilized lasers determined by frequency-comparing with an iodine-stabilized laser are 551 579 743.51 ± 0.15 MHz and 551 580 759.54 ± 1.17 MHz for ^{20}Ne and ^{22}Ne lasers, respectively. The larger uncertainty for the ^{22}Ne laser is due to fewer data points. We also investigated the effects of the weak magnetic field applied to eliminate the polarization flipping and the size of modulation depth on the locked frequency. No significant frequency shift was noticed.

Since the lineshape is asymmetric, the frequency of the Lamb-dip stabilized laser is not the frequency of the true Lamb-dip center. The asymmetry in the lineshape of Lamb-dip is investigated to deduce the true Lamb-dip center frequency. We define the asymmetry of the Lamb-dip as $\Delta_{asym} = (f_{ab} - f_{bc})/f_{ac}$, where f_{ab} stands for the frequency difference between the zero-crossing points a and b (refer to Fig. 3), and similar definition for f_{bc} and f_{ac}. We find that the asymmetry in the Lamb dip of ^{20}Ne laser is $\Delta_{asym} = +0.02$, whereas the asymmetry in the ^{22}Ne laser is $\Delta_{asym} = +0.16$. That is, the Lamb-dip centers are all blueshifted by the power background stated above. The measured frequency of zero-crossing points b is thus corrected by fitting the asymmetry of the Lamb-dip using Lamb's formula with different center frequencies for the Gaussian power background and the Lorentzian Lamb-dip lineshape [2, 4, 30]. With this correction, the absolute frequencies of the true Lamb-dip center for ^{20}Ne and ^{22}Ne lasers are:

$$\nu_{20} = 551\,579\,743 \pm 1\ \text{MHz},\ \nu_{22} = 551\,580\,757 \pm 4\ \text{MHz}.$$

The larger uncertainty quoted for the ^{22}Ne laser is due to its larger asymmetry.

The frequency-positions of these two lasers relative to the recommended wavelength standard a_9 line and the suggested wavelength standard b_{10} line of iodine [19] are illustrated in

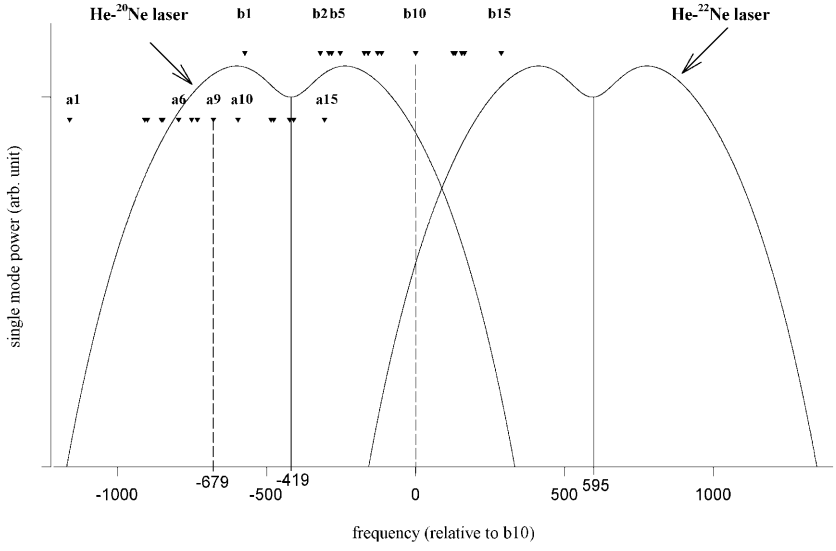

Fig. 4. The frequency positions of the Lamb-dip stabilized lasers relative to the recommended wavelength standard a_9 line and the suggested wavelength standard b_{10} line [19]. The absolute frequency of a_9 line is about 551 579 483 MHz whereas b_{10} line is about 551 580 162 MHz [28]

Fig. 4. We can find that, though the b_{10} line is a better candidate for the wavelength standard [19], its frequency is at the blue wing of the ^{20}Ne laser and at the red wing of the ^{22}Ne laser. Therefore, it is not easy to reach the b_{10} line using a pure ^{20}Ne or ^{22}Ne laser. From our experiences a laser filled with ^{20}Ne-^{22}Ne mixture is suitable for frequency stabilization to the b_{10} line of iodine.

2.3 Isotope shift

To confirm that our He-^{20}Ne and He-^{22}Ne lasers have the same filling pressure as informed by the engineer of Melles Griot, we measure the dip-width of the Lamb-dip and 199 MHz and 209 MHz are obtained for ^{20}Ne and ^{22}Ne laser, respectively. This indicates the two lasers have about the same linewidth and thus same filling pressure. Therefore, we can be sure that the pressure shift will not cause a significant systematic error in the isotope shift determination [6].

The isotope shift between ^{20}Ne and ^{22}Ne deduced is $\nu = 1014 \pm 5$ MHz, the additional uncertainty of isotope shift is caused by the slightly different pressure shift between ^{20}Ne and ^{22}Ne. It is estimated to be 2 MHz by the formula $\Delta\omega_{\text{shift}} = N \times V' \times \sigma_s$ [34]; where N denotes the number of atoms per volume, V' denotes the atomic mean relative velocity, and σ_s, about 10^{-14} cm^2 [34], corresponds to the phase shift in collision process defined in [34]. The results of the absolute frequency measurement and the isotope shift determination are summarized in Table 1 and Table 2, respectively.

The isotope shift obtained above is consistent with the work by Gerstenberger et al. [23] but has one order of magnitude better accuracy. In their work, two multi-mode 543-nm He-Ne lasers were used and 1000 ± 50 MHz isotope shift was observed directly from a Fabry–Pérot interferometer.

Table 2. The measured isotope shift

	Isotope shift
Deduced from measured frequency /MHz	1016.03 ± 1.18
Including lineshape correction /MHz	1014 ± 4
Including pressure shift uncertainty /MHz	1014 ± 5

The total isotope shift can be considered to be caused by "normal-mass-shift" (NMS) and "specific-mass-shift" (SMS) between ^{20}Ne and ^{22}Ne [35]. The NMS comes from different reduced masses and NMS $\nu_{\text{NMS}} = \nu_t \times (A' - A)/(M' \times A' \times A)$, where the atomic masses of the two isotopes are $A' = 21.9913837$ and $A = 19.9924391$ amu [36], and $M' = 1836.1527$ is the proton-to-electron-mass ratio and ν_t is the radiation frequency. For Ne $3s_2 \rightarrow 2p_{10}$ 543-nm transition, the ν_{NMS} is 1267 MHz and therefore the SMS is -253 ± 5 MHz. Such a negative SMS is consistent with the results of Kotlikov et al. and Cordoverm et al. for Ne $3s_2 \rightarrow 2p_4$ 633-nm laser transition [22, 24]. They obtained 889 ± 9 MHz and 875 ± 12 MHz isotope shift, respectively, therefore the SMS could be deduced as -284 ± 9 MHz and -298 ± 12 MHz. The obvious discrepancy between their averaged SMS (-291 ± 12 MHz) and our result (-253 ± 5 MHz) supports the J-dependence in SMS [25].

2.4 Bump in Lamb-dip

The other interesting phenomenon is, as shown in Fig. 5, a weak bump that appeared near the center of the Lamb-dip when the laser power was raised above 120 μW and two modes existed in the region of dip. It happened to all of our two-mode 543-nm He-Ne lasers filled with pure isotope.

Table 1. The measured frequencies and fitted frequencies. The uncertainties in lineshape correction come mainly from the asymmetry of lineshape (see text)

	He-^{20}Ne laser	He-^{22}Ne laser
Measured frequency /MHz	$551\,579\,743.51 \pm 0.15$	$551\,580\,759.54 \pm 1.17$
Lineshape correction /MHz	-0.5 ± 1	-3 ± 3
True dip center frequency /MHz	$551\,579\,743 \pm 1$	$551\,580\,757 \pm 4$

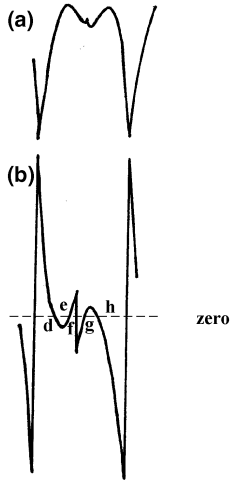

Fig. 5. a The profile of laser single-mode power for peak power > 120 μW. Here, a bump can be found near the dip-center. **b** First-harmonic signal of (**a**). Points d, e, f, g, and h are the zero-crossing points. The width of the bump is defined as frequency difference between the two zero-crossing points e and g, and 13.1 MHz is measured

Suppose the n-th mode is selected for the Lamb-dip stabilization, the bump in Lamb-dip appears when the $(n-1)$-th mode hopped out and by the mean time the $(n+1)$-th mode hopped into the wing of gain profile. This phenomenon can be monitored simultaneously by the use of a Fabry–Pérot interferometer and a chart recorder while the laser frequency is tuned increasingly across the Lamb-dip. When the laser frequency was stabilized to the peak of the bump, we find violent mode competition between the $(n+1)$-th and $(n-1)$-th modes (of the same polarization) from the Fabry–Pérot interferometer, and also the corresponding positive/negative error signal from the chart recorder. That means, half of the bump is caused by the hopping out of one mode, and the other half caused by the hopping in of the other mode. When the gain profile is narrowed by increasing the magnetic field [26], we could even observe two bumps at the symmetric position around the dip center separately. We have observed that one bump happened when the $(n-1)$-th mode hopped out, and the other happened when the $(n+1)$-th mode hopped in later. Thus we think that the bump is caused by the cross-saturation effect between two modes with weak coupling [32, 37]. However, usually only one bump can be found because of the mode competition (i.e., competition from the two side modes having the same polarization). The same phenomenon had been observed by Brand, Mensing, and Helmcke [27]. The width of such a bump is estimated to be 13.1 MHz by measuring the frequency difference between the zero-crossing points e and g in Fig. 5. Therefore, one can estimate the mode building/falling time for the $(n+1)$-th/$(n-1)$-th mode stated above (about 0.15 μs) by the formulation in [37]. Since this bump has a much narrower linewidth than the Lamb-dip, one order better stability could be achieved when the laser is stabilized to the positions e, g, or f in Fig. 5.

3 Conclusions

We have constructed two Lamb-dip stabilized 543-nm He-Ne lasers, and measured their stability, resettability, and absolute frequencies. The isotope shift between ^{20}Ne and ^{22}Ne is also determined. The results show that the Lamb-dip stabilized 543-nm He-Ne laser is appropriate to serve as a secondary wavelength standard. However, due to the asymmetric lineshape in the Lamb-dip and the pressure shift, larger uncertainty is quoted for the isotope shift in spite of the good stability of our lasers. Therefore, it will be worthwhile to investigate the 543-nm Ne transition using an external discharge cell, then one can determine the transition frequency of the Ne atom and the isotope shift more precisely.

Acknowledgements. The authors are grateful to Dr. P.-S. Cheng, Prof. C.-C. Chou, and Prof. T. Lin for helpful discussions. This work is supported by the National Science Council of the Republic of China under contract NSC 88-2112-M-007-042.

References

1. W.E. Lamb, Jr.: Proceedings of the Third Quantum Electronics Conference, Paris (1963)
2. W.E. Lamb, Jr.: Phys. Rev. **134**, 1429 (1964)
3. R.A. McFarlane, W.R. Bennett, Jr., W.E. Lamb, Jr: Appl. Phys. Lett. **2**, 189 (1963)
4. K. Shimoda, A. Javan: J. Appl. Phys. **36**, 718 (1965)
5. J.L. Hall: IEEE. J. Quantum Electron. **QE-4**, 638 (1968)
6. H. Sasada, O. Kubota: Appl. Phys. B **55**, 186 (1992)
7. H. Sasada, S. Takeuchi: J. Opt. Soc. Am. B **8**, 713 (1991)
8. G. Musturmota, M. Fujise: Electron. Lett. **25**, 814 (1989)
9. H. Buchia, M. Ohtsu, T. Tola: Jpn. J. Appl. Phys. **20**, L403 (1981)
10. K. Pescht, H. Gerhardt, E. Matthias: Z. Phys. A **281**, 199 (1977)
11. N. Mio, K. Tsubono: Appl. Phys. B **54**, 202 (1992)
12. U. Brand, J. Helmcke: In Proc. of the Fourth Symposium on Frequency Standards and Metrology, ed. by A. De Marchi, Ancona, Italy, Sept. 1988 (Springer, Berlin, Heidelberg 1989) pp. 467–468
13. J.-M. Chartier, S. Fredin-Picard, L. Robertsson: Opt. Commun. **74**, 87 (1989)
14. H. Simonsen, O. Poulsen: Appl. Phys. B **50**, 7 (1990)
15. BIPM Proc. Verb. Com. Int. Poids et Mesures 60, Recommendation 2 (CI-1992)
16. U. Brand: Opt. Commun. **100**, 361 (1993)
17. T. Lin, Y.-W. Liu, W.-Y. Cheng, J.-T. Shy, B.-R. Jih, K.-L. Ko.: Opt. Commun. **107**, 389 (1994)
18. H.R. Simonsen, U. Brand, F. Riehle: Metrologia **31**, 341 (1995)
19. W.-Y. Cheng, J.-T. Shy, T. Lin: Opt. Commun. **156**, 170 (1998)
20. H. Eicher, Z. Angew: Physica **22**, 380 (1967)
21. A. Szoke, A. Javan: Phys. Rev. Lett. **10**, 521 (1963)
22. R.H. Cordoverm, T.S. Jaseja, A. Javan: Appl. Phys. Lett. **7**, 322 (1965)
23. D.C. Gerstenberger, A. Drobshoff, S.C. Sheng: IEEE. J. Quantum Electron. **QE-24**, 501 (1988)
24. E.N. Kotlikvo, V.I. Tokarev: Opt. Spectrosc. **49**, 486 (1980)
25. J. Bauche, J.-C. Keller: Phys. Lett. A **36**, 211 (1971); J.C. Keller: J. Phys. B **6**, 1771 (1973)
26. J.-T. Shy, C.-R. Yang: Appl. Opt. **23**, 4977 (1989)
27. U. Brand, F. Mension, J. Helmcke: Appl. Phys. B **48**, 343 (1989)
28. T.J. Quinn: Metrologia **30**, 523 (1993/1994)
29. J.P. Tache, A. Le Floch, R. Le Naour: Appl. Opt. **25**, 2934 (1986)
30. A. Szoke, A. Javan: Phys. Rev. **145**, 137 (1966)
31. R.E. Walkup, A. Spielfiedel, D.E. Pritchard: Phys. Rev. Lett. **45**, 986 (1980)
32. W.R. Bennett: *The Physics of Gas Lasers* (Gordon and Breach, New York 1977) Chapt. 2
33. P. Cerez, S.J. Bennett: Appl. Opt. **18**, 1079 (1979); J. Helmcke, F. Bayer-Helms: IEEE Trans. Instrum. Meas. **IM-23**, 529 (1974)
34. W. Demtroder: *Laser Spectroscopy*, 2nd edn. (Springer, Berlin, Heidelberg 1992) Chapt. 3
35. J. Bauche, R.-J. Champeau: In *Advances in Atomic and Molecular Physics*, Vol. 12, ed. by D.R. Bates, B. Bederson (Academic Press, London 1974) pp. 39–83
36. K. Heiling, A. Stendel: At. Data Nucl. Data Tables **14**, 613 (1974)
37. M. Sargent III, M.O. Scully, W.E. Lamb, Jr.: *Laser Physics*, Sixth printing (Addison-Wesley, New York 1993) Chapt. 9